

Application of UV absorbance and fluorescence indicators to assess the formation of biodegradable dissolved organic carbon and bromate during ozonation

Original

Application of UV absorbance and fluorescence indicators to assess the formation of biodegradable dissolved organic carbon and bromate during ozonation / Li, Wen Tao; Cao, Meng Jie; Young, Tessor; Ruffino, Barbara; Dodd, Michael; Li, Ai Min; Korshin, Gregory. - In: WATER RESEARCH. - ISSN 0043-1354. - STAMPA. - 111:(2017), pp. 154-162. [10.1016/j.watres.2017.01.009]

Availability:

This version is available at: 11583/2669881 since: 2017-04-28T11:34:55Z

Publisher:

Elsevier

Published

DOI:10.1016/j.watres.2017.01.009

Terms of use:

This article is made available under terms and conditions as specified in the corresponding bibliographic description in the repository

Publisher copyright

Elsevier postprint/Author's Accepted Manuscript

© 2017. This manuscript version is made available under the CC-BY-NC-ND 4.0 license
<http://creativecommons.org/licenses/by-nc-nd/4.0/>. The final authenticated version is available online at:
<http://dx.doi.org/10.1016/j.watres.2017.01.009>

(Article begins on next page)

Application of UV absorbance and fluorescence indicators to
assess the formation of biodegradable dissolved organic carbon
and bromate during ozonation

Wen-Tao Li ^{a,b,*}, Meng-Jie Cao ^b, Tessoro Young ^b, Barbara Ruffino ^c, Michael
Dodd ^b, Ai-Min Li ^{a,*}, Gregory Korshin ^b

^a State Key Laboratory of Pollution Control and Resources Reuse, School of the
Environment, Nanjing University, Nanjing, 210023, China

^b Department of Civil & Environmental Engineering, University of Washington, Box
352700, Seattle, WA 98195-2700, United States

^c Department of Environment, Land and Infrastructure Engineering, Politecnico di
Torino, Corso Duca degli Abruzzi, 24 10129 Torino, Italy

CORRESPONDING AUTHOR FOOTNOTE:

Prof. Ai-Min Li
Email: liaimin@nju.edu.cn

Wen-Tao Li
Email: liwentaopa@hotmail.com; liwentaonju@163.com

1 **Abstract:**

2 This study examined the significance of changes of UV absorbance and
3 fluorescence of dissolved organic matter (DOM) as surrogate indicators for assessing
4 the formation of bromate and biodegradable dissolved organic carbon (BDOC) during
5 the ozonation of surface water and wastewater effluent. Spectroscopic monitoring was
6 carried out using benchtop UV/Vis and fluorescence spectrophotometers and a newly
7 developed miniature LED UV/fluorescence sensor capable of rapidly measuring
8 UVA280 and protein-like and humic-like fluorescence. With the increase of O₃/DOC
9 mass ratio, the plots of BDOC formation were characterized of initial lag, transition
10 slope and final plateau. With the decrease of UV absorbance and fluorescence, BDOC
11 concentrations initially increased slowly and then rose more noticeably. Inflection
12 points in plots of BDOC versus changes of spectroscopic indicators were close to 35-
13 45% loss of UVA254 or UVA280 and 75-85% loss of humic-like fluorescence.
14 According to the data from size exclusion chromatography (SEC) with organic carbon
15 detection and 2D synchronous correlation analyses, DOM fractions assigned to
16 operationally defined large biopolymers (apparent molecular weight, AMW>20 kDa)
17 and medium AMW humic substances (AMW 5.5-20 kDa) were transformed into
18 medium-size building blocks (AMW 3-5.5 kDa) and other smaller AMW species
19 (AMW<3 kDa) associated with BDOC at increasing O₃/DOC ratios. Appreciable
20 bromate formation was observed only after the values of UVA254, UVA280 and
21 humic-like fluorescence in O₃-treated samples were decreased by 45-55%, 50-60% and
22 86-92% relative to their respective initial levels. No significant differences in plots of

23 bromate concentrations versus decreases of humic-like fluorescence were observed for
24 surface water and wastewater effluent samples. This was in contrast with the plots of
25 bromate concentration versus UVA₂₅₄ and UVA₂₈₀ which exhibited sensitivity to
26 varying initial bromide concentrations in the investigated water matrixes. These results
27 suggest that measurements of humic-like fluorescence can provide a useful supplement
28 to UVA indices for characterization of ozonation processes.

29 **Keywords:** ozonation; biodegradable dissolved organic carbon; bromate; spectroscopic
30 indicator; humic substances; online fluorescence sensor

31 **1. Introduction**

32 Ozonation has been widely used in drinking water and wastewater treatment for
33 disinfection and oxidation purposes (Reungoat et al. 2012, von Gunten 2003a, b,
34 Zimmermann et al. 2011). Extensive studies have shown that ozonation results in
35 significant elimination of adverse biological effects of many organic micropollutants
36 (e.g., endocrine disrupting chemicals, antibiotics, and pharmaceuticals) as well as
37 removal of color, odor and taste (Dodd et al. 2009, Hollender et al. 2009, Huber et al.
38 2005, Lee et al. 2012, Liu et al. 2012a, Nakada et al. 2007, Peter and von Gunten 2007).

39 Ozone exposures required for disinfection and oxidation may result in the
40 formation of undesirable organic and inorganic byproducts, including various
41 disinfection byproducts (DBPs) and biodegradable dissolved organic carbon (BDOC)
42 (von Gunten 2003b, Wert et al. 2007). Ozonation has been shown to convert relatively
43 refractory components of dissolved organic matter (DOM) into BDOC (e.g., aldehydes,
44 carboxylic acids, ketones and etc.) without a significant decrease in overall dissolved
45 organic carbon (DOC) concentration (Liu et al. 2015, Nishijima et al. 2003, Wert et al.
46 2007). The ozonation-derived BDOC in turn largely defines the biological stability of
47 ozonated water, as it can contribute to increases in bacterial regrowth in drinking water
48 distribution systems or wastewater effluent receiving waters (Escobar and Randall
49 2001). As a result, ozonation is usually combined with a subsequent process of
50 biological filtration to consume BDOC before the treated water is conveyed into a
51 distribution system or a receiving water body. In this context, characterization of
52 changes of molecular weights (MW) of DOM and evaluation of BDOC formation may

53 provide a better understanding of integrated O₃ biofiltration processes for DOC removal.

54 In addition, ozonation of bromide-containing water or wastewater leads to the
55 formation of bromate (von Gunten and Oliveras 1998). Bromate is classified as a
56 probable or likely human carcinogen, and many countries have established the
57 maximum allowable level of bromate in drinking water at 10 µg/L (Butler et al. 2005).
58 Unlike many organic DBPs, bromate is relatively stable and is difficult to remove using
59 conventional treatment technologies (Butler et al. 2005, Nie et al. 2014). Although
60 ecological impacts of bromate formation during wastewater ozonation are uncertain,
61 the potential public health implications of bromate formation in potable water reuse
62 scenarios utilizing ozonation could be significant. Hence it is of substantial interest to
63 develop tools for better predicting and controlling bromate concentrations formed
64 during both drinking water and wastewater ozonation.

65 The formation of BDOC and bromate, as well as the elimination of micropollutants,
66 are directly related to the ozone exposure ($\int_0^t [O_3] dt$); that is, the time-dependent ozone
67 concentration integrated over exposure time. An optimization of the ozone exposure is
68 necessary to maximize the effect of oxidation and minimize the formation of undesired
69 DBPs, especially BrO₃⁻. However, for wastewater effluents, it is difficult to measure a
70 dissolved O₃ residual during the initial O₃ demand stage (Gerrity et al. 2012, Wert et al.
71 2009). Additionally, direct analyses of BDOC and bromate are time-consuming and
72 expensive. Therefore, the development of surrogate parameters for frequent online
73 monitoring to enable more automated controls of ozone dosage is warranted. For
74 example, the California Department of Public Health recently published a revised set

75 of draft regulations for groundwater replenishment, which requires full advanced
76 treatment facilities to identify at least one surrogate parameter that can be monitored
77 continuously (Chon et al. 2015, Gerrity et al. 2012).

78 A number of studies have examined the performance of spectroscopic indicators,
79 such as color, differential UV absorbance (UVA) and/or total fluorescence, and shown
80 that such indicators were correlated with the removal efficiencies of organic
81 micropollutants during ozonation (Gerrity et al. 2012, Li et al. 2016b, Liu et al. 2012b,
82 Nanaboina and Korshin 2010, Wert et al. 2009). Recently, Chon et al. (2015) applied
83 the concept of electron donating capacity of DOM combined with UVA254
84 measurements to evaluate the degradation of micropollutants and the formation of
85 bromate. Other studies have assessed the use of UVA254 and related indices to quantify
86 the formation of individual ozonation byproducts associated with BDOC (Liu et al.
87 2012a).

88 Measurements of UV absorbance at 280 nm by means of UV light emitting diodes
89 (LEDs) provide an attractive, energy-efficient alternative to conventional UVA254
90 monitoring (Bridgeman et al. 2015, Tedetti et al. 2013). UVA280 has previously been
91 found to correlate well with DOM molecular weight and aromaticity and exhibit lower
92 spectral overlap than UVA254 with inorganic species such as NO_3^- and NO_2^- that may
93 interfere with measurements in many waters (Chin et al. 1994). In addition,
94 measurements of DOM fluorescence at selected excitation and emission wavelengths
95 provide a useful complement to UVA280 since fluorescence detection can also be
96 implemented using LEDs and can enable more selective monitoring of chemically

97 reactive protein-like and humic-like DOM components (Fimmen et al. 2007, Henderson
98 et al. 2009). We recently demonstrated the use of a miniaturized LED UV/fluorescence
99 sensor – capable of online measurement of UVA280, as well as protein-like and humic-
100 like fluorescence – to predict DBP formation during chlorination (Li et al. 2016a).

101 The present study employs a sensor of this type to determine whether UVA280 and
102 fluorescence indices may be used to develop correlations with BDOC and bromate
103 formed during the ozonation of surface water and wastewater. To this end, degradation
104 of DOM chromophores and fluorophores, MW changes, and formation of BDOC and
105 bromate were examined during ozonation of a set of surface water and wastewater
106 matrixes with varying initial bromide concentrations.

107 **2. Material and methods**

108 **2.1. Water matrixes and reagents**

109 Three water matrixes were used in the experiments described below. Secondary
110 municipal wastewater effluent samples were taken from the West Point Treatment Plant
111 in King County, WA (WWTP-I on Dec 14th, 2015 and WWTP-II on Feb 28th, 2016).
112 This plant uses high-rate oxygen activated sludge technology without denitrification.
113 The surface water was sampled from Lake Pleasant, which is a brown water eutrophic
114 lake in Bothell, WA. Basic water characteristics of these waters are shown in **Table 1**.
115 All the water samples were immediately filtered through a 0.45 µm membrane upon
116 collection and stored at 4 °C before use.

117 The following chemicals were used in this study: sodium bromide (Sigma-

118 Aldrich, >99%), sodium bromate (Sigma-Aldrich, >99%), polyethylene glycol
119 standards (Alfa Aesar), methylamine solution (Sigma-Aldrich, 40 wt. % in H₂O), and
120 potassium indigotrisulfonate (Sigma-Aldrich).

121 **2.2. Ozonation batch experiments**

122 Five semi-batch ozonation experiments were performed at room temperature (25
123 ± 2 °C) with the three water matrixes mentioned above to explore the formation of
124 BDOC and bromate and evolution of spectroscopic indices during exposure to ozone.
125 For the WWTP-I water matrix (DOC 5.82 mg/L), three semi-batch experiments were
126 undertaken with spiked bromide concentrations of 50 $\mu\text{g/L}$ (WWTP-A, 322.9 $\mu\text{g/L}$ total
127 Br^-), 100 $\mu\text{g/L}$ (WWTP-B, 373.8 $\mu\text{g/L}$ total Br^-) and 200 $\mu\text{g/L}$ Br^- (WWTP-C, 491.6
128 $\mu\text{g/L}$ total Br^-) respectively, to explore effects of initial Br^- concentration. For the
129 WWTP-II water matrix (DOC 6.93 mg/L), one ozonation semi-batch experiment was
130 performed using a 100 $\mu\text{g/L}$ Br^- spike (WWTP-D, 301.5 $\mu\text{g/L}$ total Br^-) as a comparison
131 with the WWTP-I experiments. Because Lake Pleasant water had a high DOC
132 concentration (14.87 mg/L), the water was diluted 2.5 times with Milli-Q water and
133 spiked with 100 $\mu\text{g/L}$ Br^- (LP, 5.98 mg/L DOC and 116.1 $\mu\text{g/L}$ total Br^-).

134 Ozone was generated by an oxygen-fed ozonator (IN USA AC-2025; Norwood,
135 MA, USA). The feed gas stream containing ozone was bubbled through 200 mL WWTP
136 effluent or 250 mL LP water samples contained in a 500 mL borosilicate glass gas-
137 washing bottle using a sintered glass gas diffuser at a flow rate of ~ 550 ml/min. In each
138 batch experiment, the ozone doses were varied as a function of ozonation times which

139 were 0, 2, 5, 10, 15, 20, 25*, 30, 40, 50*, 60, 100, 180 and 300** s (* specific for LP
140 series and ** specific for WWTP series). The residual O₃ concentrations in ozonated
141 samples were immediately measured according to the standard indigo method (Bader
142 and Hoigné 1981), where 1 mL of ozonated sample was immediately spiked into glass
143 vials containing 9 mL indigo solution, and then analyzed for residual absorbance at 600
144 nm by UV-Vis spectroscopy. The remainder of the ozonated sample volumes was
145 transferred into 250 mL glass bottles with caps. UVA and fluorescence indicators were
146 measured at least 2 hours after ozonation, allowing the residual ozone to naturally decay
147 without adding any quenching agent. Then the samples were stored at 4 °C before other
148 analyses, which were done within 5 days for each batch.

149 Compared with directly spiking aliquots of ozone stock (Chon et al. 2015, Gerrity
150 et al. 2012), the semi-batch ozonation experiment has no dilution effect on the samples,
151 which facilitates the measurement of BDOC. However, the determination of ozone dose
152 becomes another important issue, as the rate of ozone mass transferred into water phase
153 may change as a function of time. As shown in **Figure S1**, the transferred/absorbed
154 ozone concentrations as a function of time were calculated based on measurements of
155 the differential O₃ concentrations between the feed gas and off-gas streams, where the
156 gaseous O₃ concentrations were measured by the modified indigo method (Chiou et al.
157 1995).

158 **2.3. Batch biodegradation experiments**

159 BDOC measurements were performed by quantifying the gross amount of DOC

160 degraded by an inoculum of suspended activated sludge over a predetermined period of
161 time (Escobar and Randall 2001). In this study, a requisite amount of activated sludge
162 from a WWTP was initially acclimated with glucose for 3 days. The acclimated
163 activated sludge was washed by centrifugation and resuspended in deionized water 5
164 times prior to harvesting for BDOC measurements. Then 50 mL centrifuge tubes were
165 filled with 40 ml water samples and spiked with 1 mL of the harvested activated sludge.
166 The BDOC tests were conducted in duplicate and compared with results obtained using
167 Milli-Q water as a blank control. A 200 mg/L dry biomass concentration was used in
168 the tests. This dose was determined by weighing the biomass collected from ten test
169 tubes after BDOC experiments; the biomass was dried at 105 °C before weighing. The
170 inoculated centrifuge tubes were placed in an incubated shaker at 90 rpm and 25 °C for
171 a period of 4 hours, following which the samples were centrifuged and the supernatants
172 filtered through a 0.45µm PTFE filter for subsequent DOC and molecular weight
173 analysis. The measured BDOC reflects the rapidly biodegradable fraction of BDOC
174 that can be effectively removed by biofiltration; this fraction is thus referred to as
175 BDOC_{rapid} henceforth (Black and Berube 2014).

176 **2.4. UV absorbance and fluorescence analysis**

177 A HORIBA Aqualog spectrometer was used to simultaneously measure
178 fluorescence EEM (Ex 220-450 nm / Em 245-825 nm) and UV absorbance spectra
179 (220-450 nm). The samples' EEMs were automatically corrected for Raman scattering
180 by subtracting the EEM of the water blank from the EEM of any surface water or
181 wastewater sample. Inner filter effects were corrected using the instrument's software

182 that utilized applicable absorbance data.

183 The prototype LED UV/fluorescence sensor described in more detail in (Li et al.
184 2016a) uses a UV LED (280 ± 5 nm) as a light source and a photodiode to measure the
185 intensity of light passing the cuvette. For fluorescence detection, the sensor uses blue
186 light sensitive photodiodes combined with bandpass filters (330-355 nm and 415-490
187 nm) positioned at 90° relative to the excitation beam to detect the protein-like and
188 humic-like fluorescence, respectively. Inner filter effects in fluorescence signals
189 detected by the sensor were corrected using the UVA280 values.

190 **2.5. Molecular weight analysis**

191 Analyses of DOC molecular weight distributions were performed by means of size
192 exclusion chromatography with online carbon detection (SEC-OCD). These
193 measurements utilized a DIONEX Ultimate3000 high-pressure liquid chromatography
194 (HPLC) system coupled with an online organic carbon detector (Turbo Sievers 900
195 Portable TOC Analyzer, GE). A TOSOH Bioscience Toyopearl HW-50S size exclusion
196 column was installed to separate DOM components with varying apparent MWs. The
197 injection volume was 100 μ L, and the column was eluted with 1 mL/min phosphate
198 buffer (1.5 g/L $\text{Na}_2\text{HPO}_4 \cdot 2 \text{H}_2\text{O}$ + 2.5 g/L KH_2PO_4). Polyethylene glycol standards
199 (PEG 20 kDa, 10 kDa, 6 kDa, 4 kDa, 1.5 kDa, 600 Da and 200 Da) from Alfa Aesar
200 were used as apparent molecular weight (AMW) references. The SEC-OCD
201 chromatograms for samples from each ozonation experiment were also processed with
202 Shige software developed by Noda and Ozaki (2005) for 2D correlation analysis – the

203 goal of which was to ascertain potentially small variations of various spectra resulting
204 from external perturbations, e.g., DOM ozonation in this study (supporting information
205 **Figure S4**).

206 **2.6. Bromide and bromate Analysis**

207 Bromide concentrations were determined by means of IC-ICP-MS, using a
208 PerkinElmer Series 200 HPLC coupled with a PerkinElmer SCIEX ELAN DRC-e
209 ICP/MS Spectrometer. These analyses were done in accord with prior investigators (Shi
210 and Adams 2009).

211 Bromate concentrations were determined by means of ion chromatography with
212 MS/MS detection, using a Shimadzu Prominence LC-20 series HPLC system coupled
213 with an API 4000 QTrap hybrid triple quadrupole/linear ion trap mass spectrometer
214 (AB SCIEX) operating with negative mode electrospray ionization. Separations were
215 performed using an ion exchange column (2 × 250 mm Dionex IonPac AS-16 w/ 2 ×
216 50 mm AG-16 guard column) under isocratic conditions, with a mobile phase
217 comprising 20% of a 1 mol/L aqueous methylamine solution and 80% of acetonitrile,
218 at a flow rate of 0.25 mL/min and injection volume of 100 µL. The mass parameters
219 used in multiple reaction monitoring mode for BrO₃⁻ identification and quantification
220 were 128.9→113.0 and 126.9→110.8. Method detection and quantification limits for
221 BrO₃⁻ were 0.03 and 0.1 µg/L, respectively.

222 **3. Results and discussion**

223 **3.1. Degradation of chromophores**

224 Absorbance spectra of water and wastewater ozonated at varying O_3/DOC ratios
225 normalized by the original samples' absorbance spectra are shown in **Figure 1** and
226 **Figure S2**. At all wavelengths > 230 nm, these spectra showed a monotonic decrease
227 of absorbance associated with the increase of ozone dosage. Consistent with previous
228 results (Chon et al. 2015, Gerrity et al. 2012), the normalized absorbance spectra were
229 relatively flat in the wavelength range >250 nm. The flat region in the normalized
230 absorbance spectra could be separated into sub-ranges below ~ 350 nm and above ~ 370
231 nm. At low ozone doses ($O_3/DOC < 0.4$), the observed variations of the normalized
232 absorbance at $\lambda < 350$ nm were less pronounced than those of the relative residual
233 absorbance at $\lambda > 370$ nm, and such relationships then reversed at the higher O_3/DOC
234 ratios. This phenomenon indicates that the chromophores comprise at least two
235 kinetically distinct functionalities during ozonation (Nanaboina and Korshin 2010).
236 Due to its relatively high absolute value, the UV absorbance in the range of 250-300
237 nm presents a more convenient option for online monitoring than absorbance at $\lambda > 300$
238 nm.

239 **Figure 2** illustrates that UVA₂₅₄ and UVA₂₈₀ represented as a function of
240 O_3/DOC ratio or ozonation time exhibit similar changes. With the increase of O_3/DOC
241 ratio, the UVA indices decreased steeply at low O_3/DOC ratios (< 0.5 mg O_3/mg DOC)
242 and then decreased more gradually at higher O_3/DOC ratios. When presented vs.
243 ozonation time, the normalized residual UVA indices decreased more steeply at the
244 initial ozonation stage (< 40 s) and more gradually for longer ozonation times. This
245 phenomenon could be explained by the contributions of kinetically different groups of

246 chromophores and also changes of the ozone transfer rate which varied as a function of
247 time (**Figure S1**). The O₃/DOC ratios related to such inflection points were in the range
248 of 0.4-0.6 mg O₃/mg DOC. At these O₃/DOC ratios, UVA254 and UVA280 were
249 decreased by about 45-60 %. Given that the observed changes of the absorbance of
250 ozonated water were similar for the two examined wavelengths, it can be concluded
251 that measurements at 280 nm – a practically implementable LED emission wavelength
252 feasible for online applications – may represent an excellent alternative to UVA254
253 measurements in the context of evaluation of ozonation efficiency as well as DBP
254 formation during chlorination (Li et al. 2016a).

255 **3.2. Degradation of fluorophores**

256 Representative fluorescence excitation-emission matrixes (EEM) of untreated
257 wastewater and surface water samples are shown in **Figure 3**. Generally, the
258 fluorescence peaks with Em<380 nm are ascribed to protein-like fluorescence while the
259 fluorescence peaks with Em>380 nm are ascribed to humic-like fluorescence associated
260 with fluorophores comprising aromatic rings substituted with various electron-donating
261 functional groups (Barsotti et al. 2016, Li et al. 2013, Li et al. 2015).

262 The examined wastewater samples showed the presence of two protein-like
263 fluorescence peaks (Em ~ 350 nm) and two humic-like fluorescence peaks (Em ~ 430
264 nm), while the EEM of Lake Pleasant water was dominated by two humic-like
265 fluorescence peaks (Em ~ 450 nm). The comparison of the fluorescence data obtained
266 with the LED sensor and the lab benchtop spectrometer (**Table S1**) indicates a very

267 good convergence of these results and thus confirms the good sensitivity and accuracy
268 of the LED sensor for use in online monitoring applications. However, the sensitivity
269 of the LED sensor to humic-like fluorescence is much higher than to protein-like
270 fluorescence, mainly due to the fluorescence integration area, the transmittance
271 efficiency of the sensor's bandpass filter, and the response sensitivity of photodiodes to
272 UV light. Due to the relatively weak contribution of protein-like fluorescence in Lake
273 Pleasant samples, measurements of humic-like fluorescence are mainly discussed
274 hereafter.

275 **Figure 4** illustrates the degradation of humic-like fluorophores during ozonation.
276 The humic-like fluorescence decreased very steeply at the initial stage of ozonation
277 time (< 25 s) and then reached to a distinguishable flat region at high ozone time. Like
278 for UVA254 and UVA280, the decrease of humic-like fluorescence as a function of
279 O_3/DOC ratio could also be divided into two stages; however, more than 80% of the
280 humic-like fluorescence was lost in the initial stage – much higher than for the UVA
281 indices. The O_3/DOC ratios related to such inflection points between these two stages
282 were in the range of 0.3-0.4.

283 **3.3. Formation of BDOC**

284 **Figure 5a** presents the formation of $BDOC_{\text{rapid}}$ as a function of O_3/DOC ratio or
285 ozonation time. These data demonstrate that the formation of $BDOC_{\text{rapid}}$ increased
286 gradually at O_3/DOC ratios < 0.4 and while it increased more steeply for O_3/DOC ratios
287 0.4-0.7. Above the latter transitional range of O_3/DOC ratios, $BDOC_{\text{rapid}}$ formation
288 leveled off with distinguishable plateaus at higher O_3/DOC ratios, suggesting that the

289 remaining DOM is relatively refractory and requires more O₃ to be converted to the
290 biodegradable form. Similar patterns of BDOC formation at low O₃ doses were
291 observed in prior studies. For instance, Win et al. (2000) found that the biodegradability
292 of DOM was not appreciably affected by ozonation until a threshold of ozone dose was
293 reached. Liu et al. (2015) reported that there was no significant formation of aldehydes
294 and carboxylic acids that comprise a large part of the assimilable organic carbon (AOC)
295 in ozonated wastewater (DOC 7.8 mg/L) with O₃ dose less than 2 mg/L. The plateau in
296 BDOC_{rapid} formation at higher O₃/DOC ratios is also consistent with prior observations
297 (Siddiqui et al. 1997, Treguer et al. 2010). When represented as a function of the
298 decrease of UV absorbance and fluorescence (**Figure 5b&c**), the BDOC_{rapid}
299 concentrations increased slowly in the initial stage and then rose more noticeably. The
300 inflection points in these plots corresponding to the decrease of UVA indices and
301 fluorescence were close to 35-45%, and 75-85%, respectively.

302 The degradation of DOM during ozonation can occur through either direct reaction
303 with O₃, or with [•]OH radical generated during O₃ decomposition (von Gunten 2003a,
304 Wert et al. 2009). During the initial ozone demand stage (**Figure S3**), ozone reacts
305 directly and selectively with electron-rich moieties, e.g., aromatic chromophores or
306 fluorophores (Chon et al. 2015, Wert et al. 2009, Wu et al. 2016), resulting in the rapid
307 decreases of UV absorbance and fluorescence signals (**Figure 2** and **Figure 4**). Prior
308 research based on ozonation experiments (DOC 1.2-1.4 mg/L, O₃ 2 mg/L) performed
309 with and without [•]OH scavengers confirmed that direct ozone reactions are mainly
310 responsible for the formation of small organic compounds contributing to AOC during

311 the initial ozone demand stage (Hammes et al. 2006). However, such AOC molecules
312 might not be produced substantially at very low ozone dose (Liu et al. 2015). In the
313 present work, it is possible that the initial selective attacks of O₃ on electron-rich
314 moieties were not sufficient to break down the large MW DOM fractions into small
315 molecules associated with AOC, leading to the apparent lag in formation of BDOC_{rapid}
316 at O₃/DOC ratios < 0.4. The presence of small quantities of inorganic constituents that
317 might exert rapid O₃ demand at low O₃ doses (e.g., NO₂⁻) also cannot be ruled out. With
318 greater O₃ doses, increasing exposure to O₃ and [•]OH may have led to more extensive
319 breakdown of aromatic structures and other electron-rich targets through direct
320 reactions with O₃ and indirect reactions involving the much less selective [•]OH (Legrini
321 et al. 1993, von Gunten 2003a). At O₃/DOC ratios above 0.4-0.7, the observed decrease
322 in formation of BDOC_{rapid} may be attributable to accumulation of more O₃- and [•]OH-
323 recalcitrant products (e.g., acetic and oxalic acids) (Hammes et al. 2006, Ramseier and
324 Gunten 2009). The synergistic effect of O₃ and [•]OH radical contributed to the sufficient
325 decomposition of large MW DOM and the prominent formation of AOCs.

326 **3.4. Evolution of DOM molecular weight during ozonation**

327 **Figure 6** shows the evolution of SEC-OCD chromatograms of WWTP effluent and
328 Lake Pleasant water during ozonation. In SEC experiments, DOM fractions with higher
329 apparent MW have lower elution times (**Figure S4**). Using peak assignments
330 introduced in prior research (Huber et al. 2011) to denote major features observed in
331 the data shown in **Figure 6**, both WWTP effluent and Lake Pleasant water had a
332 biopolymer-like peak of large AMW (peak a1 and peak b1, 20-30 min, AMW > 20

333 kDa). The WWTP effluent exhibited several peaks in the medium AMW range (peak
334 a2, humic-like peak, 30-36 min, AMW of 14-5.5 kDa; peak a3, peak of building blocks,
335 36-40 min, AMW of 5.5-3 kDa) and two well-resolved peaks located at lower AMW
336 values (peak a4, peak of low MW acids, 40-48 min, AMW of 3-0.8 kDa; peak a5, peak
337 of low MW neutrals, 50-60 min, AMW < 800 Da). SEC-OCD data for Lake Pleasant
338 water exhibited a prominent peak b2 (humic-like peak, 28-36 min, AMW of 20-5.5 kDa)
339 with a shoulder b3 (building blocks, 36-40 min, AMW of 5.5-3 kDa). These peaks
340 located in the range of medium AMW typically attributed to humic substances were
341 responsible for a large portion of DOC in untreated Lake Pleasant water. The SEC-
342 OCD of Lake Pleasant water also had two weaker peaks located in the range of small
343 AMW (peak b4 and peak b5), which are designated as low MW acids and neutrals.

344 The evolution of apparent DOM molecular weights is indicated by the red arrows
345 in **Figure 6**. It is also visualized using 2D synchronous correlation contours (**Figure**
346 **S5**). At increasing ozone dosages, the large MW biopolymer-like peaks (a1 and b1) and
347 medium MW humic-like peaks (a2 and b2) decreased while the concentration of
348 building blocks and low MW acids and neutrals increased, suggesting that the larger
349 AMW DOM components were transformed into smaller AMW species during
350 ozonation. The newly formed medium building blocks and small MW DOM species
351 were easily biodegraded and mainly contributed to the BDOC_{rapid} (**Figure S6**). The
352 SEC-OCD results also confirmed that the decomposition of biopolymer-like or humic-
353 like peaks was not prominent (<20%) during the initial ozonation stage, despite the
354 substantial losses of UVA and fluorescence (**Figure S7**).

355 3.5. Formation of bromate

356 **Figures 7a-b** depict bromate yields (expressed as mol ratios of Br associated with
357 BrO_3^- to initial Br^- ($[\text{BrO}_3^-]/[\text{Br}^-]$, in % mol/mol) plotted as a function of O_3/DOC ratio
358 or ozonation time. The observed relationships exhibit the presence of two phases of
359 bromate formation, as marked by the dash line. During the initial phase (O_3/DOC ratios
360 < 0.4 or ozonation time < 25 s), bromate yields were low ($[\text{BrO}_3^-]/[\text{Br}^-] < 2$ %) and
361 effects of initial Br^- concentrations on this phase were minor. This is in agreement with
362 the data of previous studies (Chon et al. 2015, Soltermann et al. 2016), which observed
363 a negligible bromate yield ($\leq 3\%$) for O_3/DOC ratios < 0.4 - 0.6 mg O_3/mg DOC.

364 This phenomenon can be ascribed to specific features of the formation pathway of
365 bromate, which is generated via a complex mechanism involving ozone and hydroxyl
366 radical (Fischbacher et al. 2015, von Gunten and Oliveras 1998). During the initial
367 phase of bromate formation (O_3/DOC ratios < 0.4 , ozonation time < 25 s), O_3 is rapidly
368 consumed by electron-rich moieties (Buffle et al. 2006, Lee et al. 2013) whose
369 consumption is consistent with the rapid decrease of humic-like fluorescence (**Figure**
370 **4**), thus leaving little residual O_3 for reaction with Br^- (**Figure S3**). In the second phase,
371 in which measured residual ozone concentrations exceeded 1 mg/L (**Figure S3**),
372 bromide could be readily oxidized to bromate, with its yields increasing with the ozone
373 doses, and different water matrixes had a significant effect on the bromate yields
374 measured as a function of O_3/DOC ratio or ozonation time.

375 When plotted versus O_3/DOC ratio, the bromate formation across different water

376 matrixes was similar for each matrix when presented in terms of bromate concentration
377 in $\mu\text{g/L}$ (**Figure S8**), but different when represented in terms of bromate yield units
378 (**Figure 7**). That is, the lower initial bromide concentration in Lake Pleasant water led
379 to higher molar bromate yields compared to those for the higher-bromide WWTP
380 effluent samples at the same ozone doses. Compared with the data of the previous study
381 (Chon et al. 2015), the bromate formation yields of WWTP effluent samples at the
382 corresponding O_3/DOC ratios in the present work were lower, possibly due to the higher
383 initial Br^- concentrations in this study (Br^- 300-500 $\mu\text{g/L}$ for DOC 5.8-6.9 mg/L vs. Br^-
384 39-86 $\mu\text{g/L}$ for DOC 5.3-7.3 mg/L). Therefore, the O_3/DOC ratio might not always be
385 an optimal indicator for estimation of bromate formation across different water matrixes.

386 **Figures 7c-d** present the normalized bromate yields ($[\text{BrO}_3^-]/[\text{Br}^-]$, mol/mol) as a
387 function of relative changes in the spectroscopic parameters UVA254, UVA280 and
388 humic-like fluorescence. In agreement with one previous study (Chon et al. 2015), the
389 plots of bromate yields vs. spectroscopic indicators overlapped for all data sets obtained
390 in the ozonation experiments, although the DOM properties and initial Br^-
391 concentrations were different. Similarly to the observations discussed above, changes
392 in the bromate yields could be further divided into two stages characterized by
393 significantly different slopes vs. corresponding spectroscopic index. The inflection
394 points related to the appreciable formation of BrO_3^- were in the range of 45-55%, 50-
395 60% and 86-92% losses of UVA254, UVA280, and humic-like fluorescence,
396 respectively. Unlike O_3/DOC ratios, the plots of $[\text{BrO}_3^-]/[\text{Br}^-]$ as a function of the
397 spectroscopic indicators in the second phase had relatively small differences for the

398 data obtained for Lake Pleasant and WWTP effluent samples, suggesting that the
399 spectroscopic indices may be more suitable as a surrogate parameter for bromate
400 formation in waters of varying composition.

401 With respect to the US EPA's MCL for BrO_3^- in drinking water of $10 \mu\text{g/L}$, the
402 breakthrough points related to removals of UVA254, UVA280 and decrease of humic-
403 like fluorescence were in the range of 45-55%, 52-57%, and 86-90%, respectively
404 (**Figure 8**). In contrast to the observations made for $[\text{BrO}_3^-]/[\text{Br}^-]$ molar yields (**Figure**
405 **7**), plots of BrO_3^- vs UVA254 and BrO_3^- vs UVA280 diverged into distinct groups of
406 data for WWTP effluents and Lake Pleasant. Such divergences were presumably due
407 to differences in initial Br^- concentrations in the various matrixes, since BrO_3^- yields
408 were not normalized to initial Br^- levels in these plots. Additionally, chromophores in
409 Lake Pleasant water appeared to be much more susceptible to the oxidation at higher
410 O_3 exposures than chromophores in WWTP effluents (**Figure 2**). However, no
411 significant divergences between the data for dissimilar water matrixes were observed
412 in plots of BrO_3^- vs humic fluorescence. In comparison to the ~25% variation amongst
413 UVA indices in the various matrixes at higher O_3 exposures, further decreases of
414 humic-like fluorescence were limited in a narrow range from 90% to 100%. The
415 association of this narrow range of changes of humic-like fluorescence with the
416 generation of bromate is likely to have largely eliminated any divergence attributable
417 to differences in initial Br^- concentration. A previous study also reported a sole
418 correlation between a fluorescence index and several chlorinated DBPs regardless of
419 the water source and treatment, while the differential absorbance correlations could be

420 interfered by many species (Roccaro et al. 2009). These results showed that
421 fluorescence indices may have more advantages than absorbance indices in actual water
422 systems.

423 The plots of BrO_3^- concentration ($\mu\text{g/L}$) versus decrease of humic fluorescence (HS,
424 in %) were fitted by MATLAB software (**Figure S9**), and an empirical equation
425 applicable to the ranges of 6-7 mg/L DOC and 100-500 $\mu\text{g/L}$ Br^- was obtained, as
426 presented below:

$$427 \quad \text{BrO}_3^- (\mu\text{g/L}) = 7.64 * 10^{-9} * e^{0.237*HS(\%)} , R^2 = 0.962$$

428 The results of this study suggest that measurements of changes in humic-like
429 fluorescence of ozonated water are highly suitable for the estimation of bromate
430 formation in dissimilar water matrixes. The results in **Figure S10** further indicate that
431 DOC concentration has relatively little effect on the relationships between bromate
432 formation and humic-like fluorescence. However, the robustness of such relationships
433 still needs to be explored in the future; for example, with respect to the effects of pH,
434 temperature, DOC and NH_4^+ concentrations.

435 In the context of optimization of ozone dosage, the typical goal is to maximize the
436 effect of oxidation while simultaneously minimizing the formation of undesired
437 byproducts. Gerrity et al. (2012) previously reported that ~50% reduction of UVA254
438 or ~90% decrease of total fluorescence were required to reach acceptable levels of
439 pathogen inactivation and sufficient elimination of many micropollutants. The present
440 work supports these findings and demonstrates possible approaches for assessing the

441 potential formation of BDOC and bromate during water and wastewater ozonation,
442 especially for water having bromide concentrations above 50 µg/L.

443 **4. Conclusions**

- 444 ● When represented as a function of changes of spectroscopic indicators such as
445 UVA254, UVA280, and humic-like fluorescence, BDOC concentrations initially
446 increased slowly and then rose more noticeably. The inflection points indicative of
447 BDOC formation threshold were located in the range of 35-45% loss of UVA254
448 or UVA280 and 75-85% loss of humic-like fluorescence.
- 449 ● SEC-OCD data showed that large biopolymer molecules in WWTP effluent
450 (apparent MW>20 kDa) and medium-AMW humic substances in Lake Pleasant
451 surface water (AMW 5.5-20 kDa) were transformed into medium-AMW building
452 blocks and small AMW species associated with BDOC.
- 453 ● When represented as a function of spectroscopic indicators, the inflection points
454 that corresponded to the onset of bromate formation were approximately 45-55%,
455 50-60% and 86-92% for decreases in UVA254, UVA280 and humic fluorescence,
456 respectively.
- 457 ● An empirical equation modeling the relationship between bromate concentrations
458 (expressed in µg/L) and concomitant decreases of humic-like fluorescence (%) was
459 established based on the data generated for wastewater effluent and surface water
460 that had 100 to 500 µg/L Br⁻.
- 461 ● The results suggest that measurements of UVA280 and humic-like fluorescence

462 complement conventional UVA254 measurements, especially in the context of
463 assessing the formation of BDOC and bromate. The use of these spectroscopic
464 parameters is expected to be enhanced by the recent development of
465 online/portable spectrometers that use LEDs as a light source.

466 **Acknowledgement**

467 We thank the generous support from National Key R&D Program (No.
468 2016YFE0112300), National Science Foundation of China (No. 51438008) and
469 MADFORWATER (No. 688320) for the development of LED UV fluorescence sensor.
470 We also acknowledge the support for Tessoria Young from her NSF graduate research
471 fellowship. Wentao Li thanks the scholarship from the China Scholarship Council (No.
472 201506190059) and Shanghai Tongji GaoTingyao Environmental Science &
473 Technology Development Foundation (STGEF).

474 **Appendix A. Supplementary data**

475 Supplementary data related to this article can be found in Supporting Information.

476 **References**

- 477 Bader, H. and Hoigné, J., 1981. Determination of ozone in water by the indigo method.
478 Water Research 15 (4), 449-456.
- 479 Barsotti, F., Ghigo, G. and Vione, D., 2016. Computational assessment of the
480 fluorescence emission of phenol oligomers: A possible insight into the
481 fluorescence properties of humic-like substances (HULIS). Journal of
482 Photochemistry and Photobiology a-Chemistry 315, 87-93.
- 483 Black, K.E. and Berube, P.R., 2014. Rate and extent NOM removal during oxidation
484 and biofiltration. Water Research 52, 40-50.
- 485 Bridgeman, J., Baker, A., Brown, D. and Boxall, J.B., 2015. Portable LED fluorescence
486 instrumentation for the rapid assessment of potable water quality. Science of The
487 Total Environment 524–525, 338-346.
- 488 Buffle, M.-O., Schumacher, J., Salhi, E., Jekel, M. and von Gunten, U., 2006.
489 Measurement of the initial phase of ozone decomposition in water and wastewater
490 by means of a continuous quench-flow system: Application to disinfection and
491 pharmaceutical oxidation. Water Research 40 (9), 1884-1894.
- 492 Butler, R., Godley, A., Lytton, L. and Cartmell, E., 2005. Bromate environmental
493 contamination: Review of impact and possible treatment. Critical Reviews in
494 Environmental Science and Technology 35 (3), 193-217.
- 495 Chin, Y.-P., Aiken, G. and O'Loughlin, E., 1994. Molecular Weight, Polydispersity,
496 and Spectroscopic Properties of Aquatic Humic Substances. Environmental
497 Science & Technology 28 (11), 1853-1858.

498 Chiou, C.F., Marinas, B.J. and Adams, J.Q., 1995. Modified indigo method for gaseous
499 and aqueous ozone analyses. *Ozone-Science & Engineering* 17 (3), 329-344.

500 Chon, K., Salhi, E. and von Gunten, U., 2015. Combination of UV absorbance and
501 electron donating capacity to assess degradation of micropollutants and formation
502 of bromate during ozonation of wastewater effluents. *Water Research* 81, 388-397.

503 Dodd, M.C., Kohler, H.P.E. and von Gunten, U., 2009. Oxidation of Antibacterial
504 Compounds by Ozone and Hydroxyl Radical: Elimination of Biological Activity
505 during Aqueous Ozonation Processes. *Environmental Science & Technology* 43
506 (7), 2498-2504.

507 Escobar, I.C. and Randall, A.A., 2001. Assimilable organic carbon (AOC) and
508 biodegradable dissolved organic carbon (BDOC): Complementary measurements.
509 *Water Research* 35 (18), 4444-4454.

510 Fimmen, R.L., Cory, R.M., Chin, Y.-P., Trouts, T.D. and McKnight, D.M., 2007.
511 Probing the oxidation–reduction properties of terrestrially and microbially derived
512 dissolved organic matter. *Geochimica et Cosmochimica Acta* 71 (12), 3003-3015.

513 Fischbacher, A., Loeppenber, K., von Sonntag, C. and Schmidt, T.C., 2015. A New
514 Reaction Pathway for Bromite to Bromate in the Ozonation of Bromide.
515 *Environmental Science & Technology* 49 (19), 11714-11720.

516 Gerrity, D., Gamage, S., Jones, D., Korshin, G.V., Lee, Y., Pisarenko, A., Trenholm,
517 R.A., von Gunten, U., Wert, E.C. and Snyder, S.A., 2012. Development of
518 surrogate correlation models to predict trace organic contaminant oxidation and
519 microbial inactivation during ozonation. *Water Research* 46 (19), 6257-6272.

520 Hammes, F., Salhi, E., Koster, O., Kaiser, H.P., Egli, T. and von Gunten, U., 2006.
521 Mechanistic and kinetic evaluation of organic disinfection by-product and
522 assimilable organic carbon (AOC) formation during the ozonation of drinking
523 water. *Water Research* 40 (12), 2275-2286.

524 Henderson, R.K., Baker, A., Murphy, K.R., Hambly, A., Stuetz, R.M. and Khan, S.J.,
525 2009. Fluorescence as a potential monitoring tool for recycled water systems: A
526 review. *Water Research* 43 (4), 863-881.

527 Hollender, J., Zimmermann, S.G., Koepke, S., Krauss, M., McArdell, C.S., Ort, C.,
528 Singer, H., von Gunten, U. and Siegrist, H., 2009. Elimination of Organic
529 Micropollutants in a Municipal Wastewater Treatment Plant Upgraded with a Full-
530 Scale Post-Ozonation Followed by Sand Filtration. *Environmental Science &*
531 *Technology* 43 (20), 7862-7869.

532 Huber, M.M., Gobel, A., Joss, A., Hermann, N., Loffler, D., McArdell, C.S., Ried, A.,
533 Siegrist, H., Ternes, T.A. and von Gunten, U., 2005. Oxidation of pharmaceuticals
534 during ozonation of municipal wastewater effluents: A pilot study. *Environmental*
535 *Science & Technology* 39 (11), 4290-4299.

536 Huber, S.A., Balz, A., Abert, M. and Pronk, W., 2011. Characterisation of aquatic
537 humic and non-humic matter with size-exclusion chromatography – organic
538 carbon detection – organic nitrogen detection (LC-OCD-OND). *Water Research*
539 45 (2), 879-885.

540 Lee, C.O., Howe, K.J. and Thomson, B.M., 2012. Ozone and biofiltration as an
541 alternative to reverse osmosis for removing PPCPs and micropollutants from

542 treated wastewater. *Water Research* 46 (4), 1005-1014.

543 Lee, Y., Gerrity, D., Lee, M., Bogeat, A.E., Salhi, E., Gamage, S., Trenholm, R.A.,
544 Wert, E.C., Snyder, S.A. and von Gunten, U., 2013. Prediction of Micropollutant
545 Elimination during Ozonation of Municipal Wastewater Effluents: Use of Kinetic
546 and Water Specific Information. *Environmental Science & Technology* 47 (11),
547 5872-5881.

548 Legrini, O., Oliveros, E. and Braun, A.M., 1993. Photochemical processes for water
549 treatment. *Chemical Reviews* 93 (2), 671-698.

550 Li, W.-T., Jin, J., Li, Q., Wu, C.-F., Lu, H., Zhou, Q. and Li, A.-M., 2016a. Developing
551 LED UV fluorescence sensors for online monitoring DOM and predicting DBPs
552 formation potential during water treatment. *Water Research* 93, 1-9.

553 Li, W.-T., Xu, Z.-X., Li, A.-M., Wu, W., Zhou, Q. and Wang, J.-N., 2013.
554 HPLC/HPSEC-FLD with multi-excitation/emission scan for EEM interpretation
555 and dissolved organic matter analysis. *Water Research* 47 (3), 1246-1256.

556 Li, W., Nanaboina, V., Chen, F. and Korshin, G.V., 2016b. Removal of polycyclic
557 synthetic musks and antineoplastic drugs in ozonated wastewater: Quantitation
558 based on the data of differential spectroscopy. *Journal of Hazardous Materials* 304,
559 242-250.

560 Li, W., Xu, Z., Wu, Q., Li, Y., Shuang, C. and Li, A., 2015. Characterization of
561 fluorescent-dissolved organic matter and identification of specific fluorophores in
562 textile effluents. *Environmental Science and Pollution Research* 22 (6), 4183-4189.

563 Liu, C., Nanaboina, V. and Korshin, G., 2012a. Spectroscopic study of the degradation

564 of antibiotics and the generation of representative EfOM oxidation products in
565 ozonated wastewater. *Chemosphere* 86 (8), 774-782.

566 Liu, C., Nanaboina, V., Korshin, G.V. and Jiang, W., 2012b. Spectroscopic study of
567 degradation products of ciprofloxacin, norfloxacin and lomefloxacin formed in
568 ozonated wastewater. *Water Research* 46 (16), 5235-5246.

569 Liu, C., Tang, X., Kim, J. and Korshin, G.V., 2015. Formation of aldehydes and
570 carboxylic acids in ozonated surface water and wastewater: A clear relationship
571 with fluorescence changes. *Chemosphere* 125, 182-190.

572 Nakada, N., Shinohara, H., Murata, A., Kiri, K., Managaki, S., Sato, N. and Takada, H.,
573 2007. Removal of selected pharmaceuticals and personal care products (PPCPs)
574 and endocrine-disrupting chemicals (EDCs) during sand filtration and ozonation
575 at a municipal sewage treatment plant. *Water Research* 41 (19), 4373-4382.

576 Nanaboina, V. and Korshin, G.V., 2010. Evolution of Absorbance Spectra of Ozonated
577 Wastewater and Its Relationship with the Degradation of Trace-Level Organic
578 Species. *Environmental Science & Technology* 44 (16), 6130-6137.

579 Nie, Y., Hu, C., Li, N., Yang, L. and Qu, J., 2014. Inhibition of bromate formation by
580 surface reduction in catalytic ozonation of organic pollutants over beta-
581 FeOOH/Al₂O₃. *Applied Catalysis B-Environmental* 147, 287-292.

582 Nishijima, W., Fahmi, Mukaidani, T. and Okada, M., 2003. DOC removal by multi-
583 stage ozonation-biological treatment. *Water Research* 37 (1), 150-154.

584 Noda, I. and Ozaki, Y. (2005) Two-dimensional correlation spectroscopy: applications
585 in vibrational and optical spectroscopy, John Wiley & Sons.

586 Peter, A. and von Gunten, U., 2007. Oxidation kinetics of selected taste and odor
587 compounds during ozonation of drinking water. *Environmental Science &*
588 *Technology* 41 (2), 626-631.

589 Ramseier, M.K. and Gunten, U.v., 2009. Mechanisms of Phenol Ozonation—Kinetics
590 of Formation of Primary and Secondary Reaction Products. *Ozone: Science &*
591 *Engineering* 31 (3), 201-215.

592 Reungoat, J., Escher, B.I., Macova, M., Argaud, F.X., Gernjak, W. and Keller, J., 2012.
593 Ozonation and biological activated carbon filtration of wastewater treatment plant
594 effluents. *Water Research* 46 (3), 863-872.

595 Roccaro, P., Vagliasindi, F.G.A. and Korshin, G.V., 2009. Changes in NOM
596 Fluorescence Caused by Chlorination and their Associations with Disinfection by-
597 Products Formation. *Environmental Science & Technology* 43 (3), 724-729.

598 Shi, H. and Adams, C., 2009. Rapid IC–ICP/MS method for simultaneous analysis of
599 iodoacetic acids, bromoacetic acids, bromate, and other related halogenated
600 compounds in water. *Talanta* 79 (2), 523-527.

601 Siddiqui, M.S., Amy, G.L. and Murphy, B.D., 1997. Ozone enhanced removal of
602 natural organic matter from drinking water sources. *Water Research* 31 (12), 3098-
603 3106.

604 Soltermann, F., Abegglen, C., Götz, C. and von Gunten, U., 2016. Bromide Sources
605 and Loads in Swiss Surface Waters and Their Relevance for Bromate Formation
606 during Wastewater Ozonation. *Environmental Science & Technology* 50 (18),
607 9825-9834.

608 Tedetti, M., Joffre, P. and Goutx, M., 2013. Development of a field-portable
609 fluorometer based on deep ultraviolet LEDs for the detection of phenanthrene- and
610 tryptophan-like compounds in natural waters. *Sensors and Actuators B-Chemical*
611 182, 416-423.

612 Treguer, R., Tatin, R., Couvert, A., Wolbert, D. and Tazi-Pain, A., 2010. Ozonation
613 effect on natural organic matter adsorption and biodegradation - Application to a
614 membrane bioreactor containing activated carbon for drinking water production.
615 *Water Research* 44 (3), 781-788.

616 von Gunten, U., 2003a. Ozonation of drinking water: Part I. Oxidation kinetics and
617 product formation. *Water Research* 37 (7), 1443-1467.

618 von Gunten, U., 2003b. Ozonation of drinking water: Part II. Disinfection and by-
619 product formation in presence of bromide, iodide or chlorine. *Water Research* 37
620 (7), 1469-1487.

621 von Gunten, U. and Oliveras, Y., 1998. Advanced Oxidation of Bromide-Containing
622 Waters: Bromate Formation Mechanisms. *Environmental Science & Technology*
623 32 (1), 63-70.

624 Wert, E.C., Rosario-Ortiz, F.L., Drury, D.D. and Snyder, S.A., 2007. Formation of
625 oxidation byproducts from ozonation of wastewater. *Water Research* 41 (7), 1481-
626 1490.

627 Wert, E.C., Rosario-Ortiz, F.L. and Snyder, S.A., 2009. Using Ultraviolet Absorbance
628 and Color To Assess Pharmaceutical Oxidation during Ozonation of Wastewater.
629 *Environmental Science & Technology* 43 (13), 4858-4863.

630 Wu, Q., Li, W.T., Yu, W.H., Li, Y. and Li, A.M., 2016. Removal of fluorescent
631 dissolved organic matter in biologically treated textile wastewater by ozonation-
632 biological aerated filter. *Journal of the Taiwan Institute of Chemical Engineers* 59,
633 359-364.

634 Zimmermann, S.G., Wittenwiler, M., Hollender, J., Krauss, M., Ort, C., Siegrist, H. and
635 von Gunten, U., 2011. Kinetic assessment and modeling of an ozonation step for
636 full-scale municipal wastewater treatment: Micropollutant oxidation, by-product
637 formation and disinfection. *Water Research* 45 (2), 605-617.

638

639 **Table 1. Basic characteristics of water matrixes**

Parameters	WWTP-I	WWTP-II	Lake Pleasant
pH	6.92	6.95	7.48 ^a
DOC (mg/L)	5.82	6.93	14.87
UV254 (cm⁻¹)	0.130	0.139	0.727
UV280 (cm⁻¹)	0.100	0.108	0.545
Conductivity (us/cm)	480	652	314
Br⁻ (µg/L) ^b	267.8	201.5	36.7

^a The pH values of 2.5 times diluted lake Pleasant water were about 7.

^b The values listed here are the native background Br⁻ concentrations for each water matrix. Initial Br⁻ concentrations during ozonation batch experiments, using samples of each water matrix fortified with additional bromide, were as follows: 322.9 µg/L for WWTP-A, 373.8 µg/L for WWTP-B, 491.6 µg/L for WWTP-C, 301.5 µg/L for WWTP-D, and 116.1 µg/L for LP.

640

Figure Captions

Figure 1. Changes in the absorbance spectra of WWTP effluent as a function of O_3/DOC ratio normalized by the absorbance prior to treatment

Figure 2. Decreases of the normalized residual UVA indices as a function of O_3/DOC ratio (or ozonation time – inserts): (a) UVA254 and (b) UVA280

Figure 3. EEM spectra of (a) WWTP-I, (b) WWTP-II, and (c) LP. The circles on the left of each graph represent protein-like fluorescence that the LED sensor measures, while the circles on the right of each graph represent humic-like fluorescence that the LED sensor measures.

Figure 4. Decrease of the normalized humic-like fluorescence (H/H_0) as a function of O_3/DOC ratio or ozonation time (insert) in different ozonation experiments

Figure 5. Formation of $BDOC_{\text{rapid}}$ as a function of (a) O_3/DOC ratio or ozonation time (insert), (b) decrease of UVA254 or UVA280 (insert) and (c) decrease of LED humic-like fluorescence

Figure 6. Evolution of SEC-OCD chromatograms of the ozonated wastewater and surface water as a function of O_3/DOC ratio: (a) WWTP-I effluent (WWTP-A) and (b) Lake Pleasant water (LP).

Figure 7. Bromate formation yields ($[BrO_3^-]/[Br^-]$, mol/mol in %) represented as a function of (a) O_3/DOC ratio, (b) ozonation time, (c) decrease of UVA254 or UVA280 (insert) and (d) decrease of LED humic-like fluorescence.

Figure 8. Bromate formation ($\mu\text{g/L}$) as a function of decreases of spectral indicators: (a) UVA254 or UVA280 (insert) and (b) LED humic-like fluorescence

Figure 1

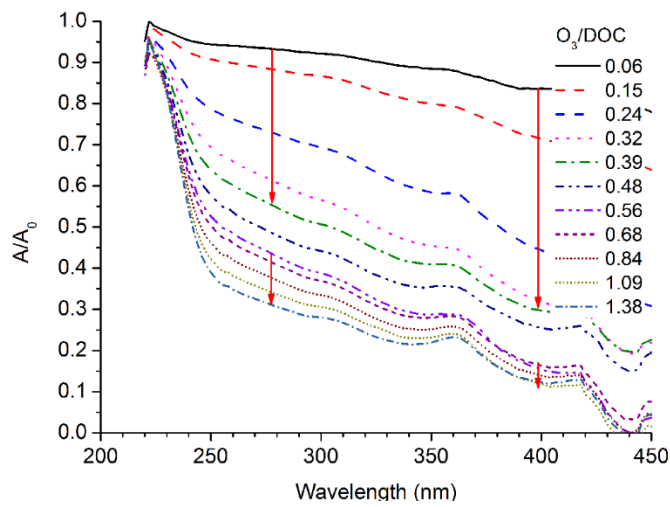


Figure 2

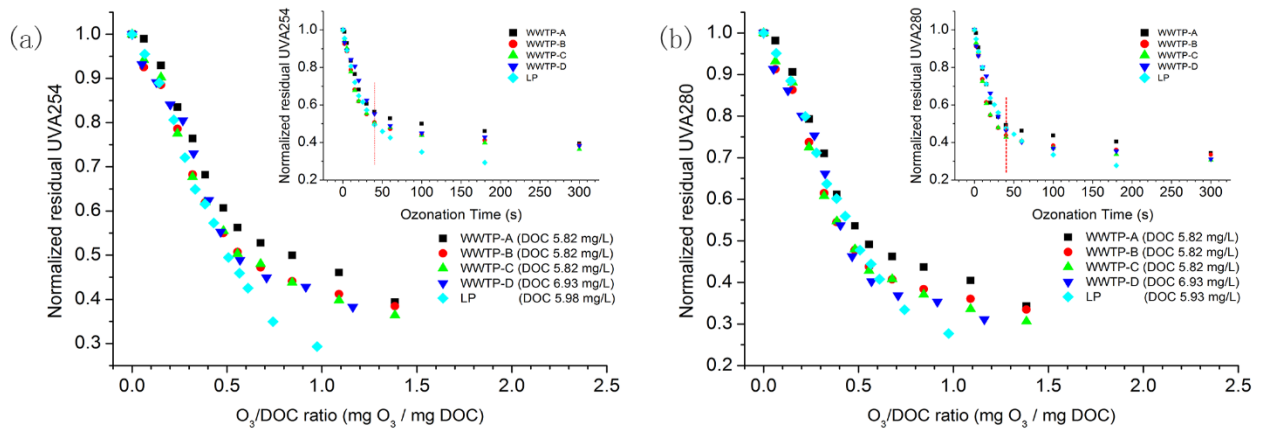


Figure 3

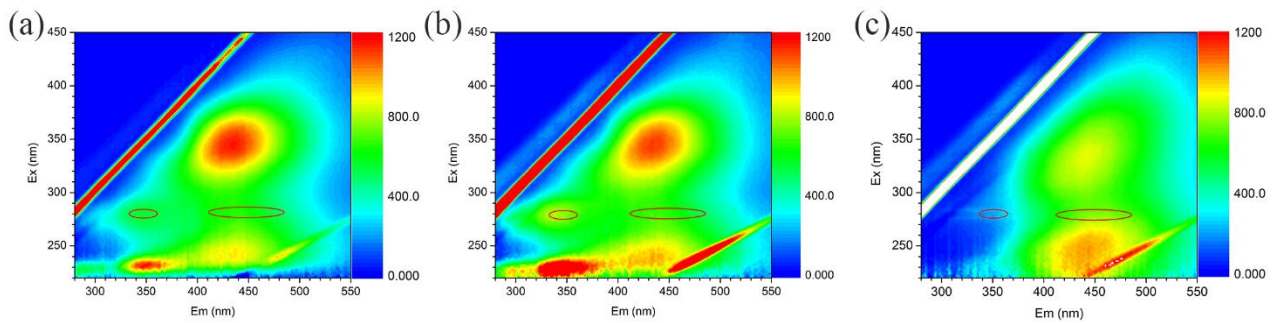


Figure 4

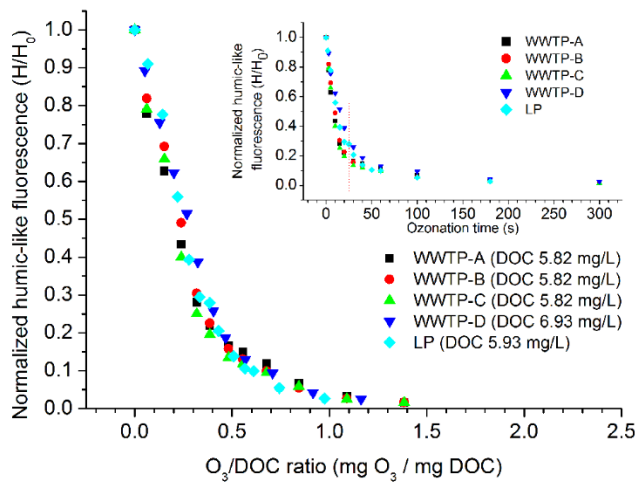


Figure 5

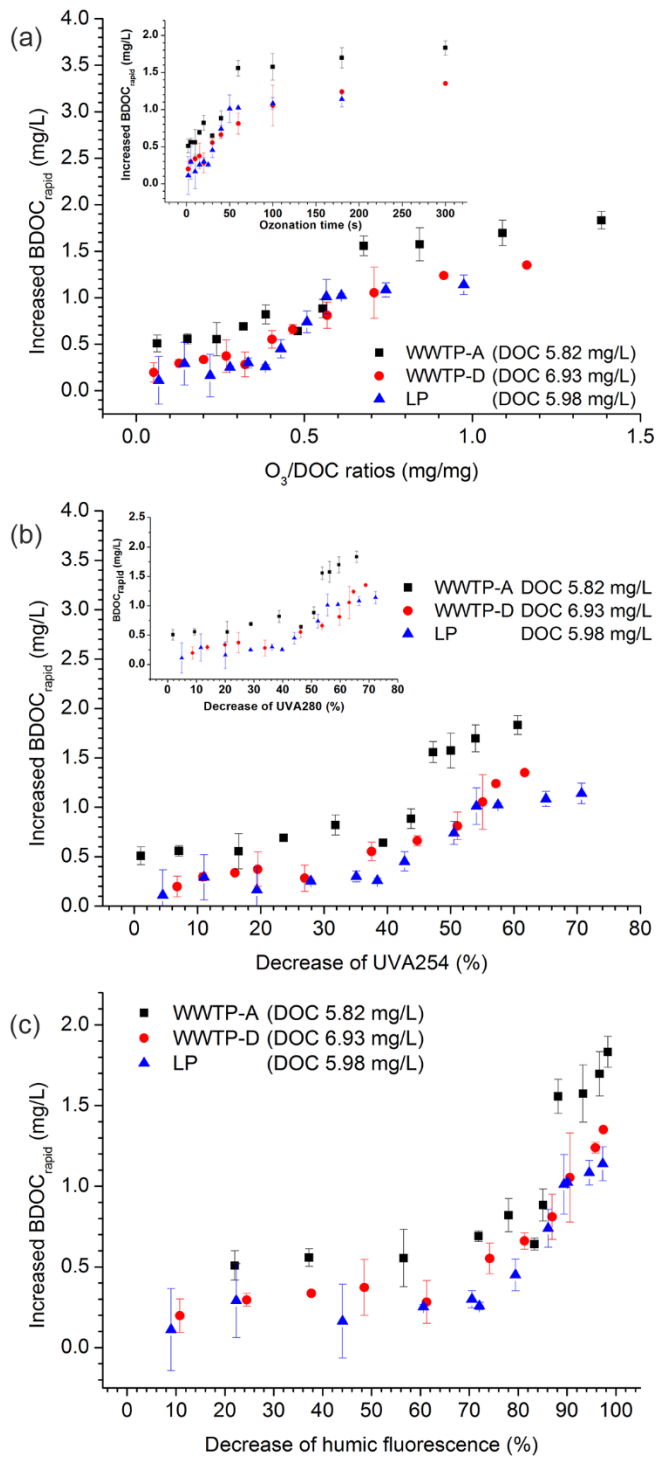


Figure 6

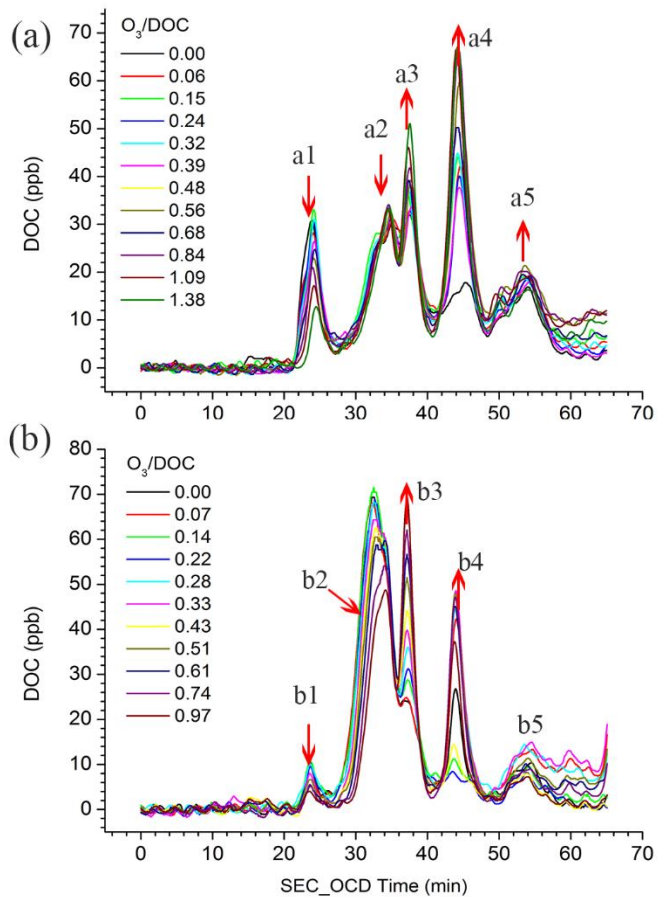


Figure 7

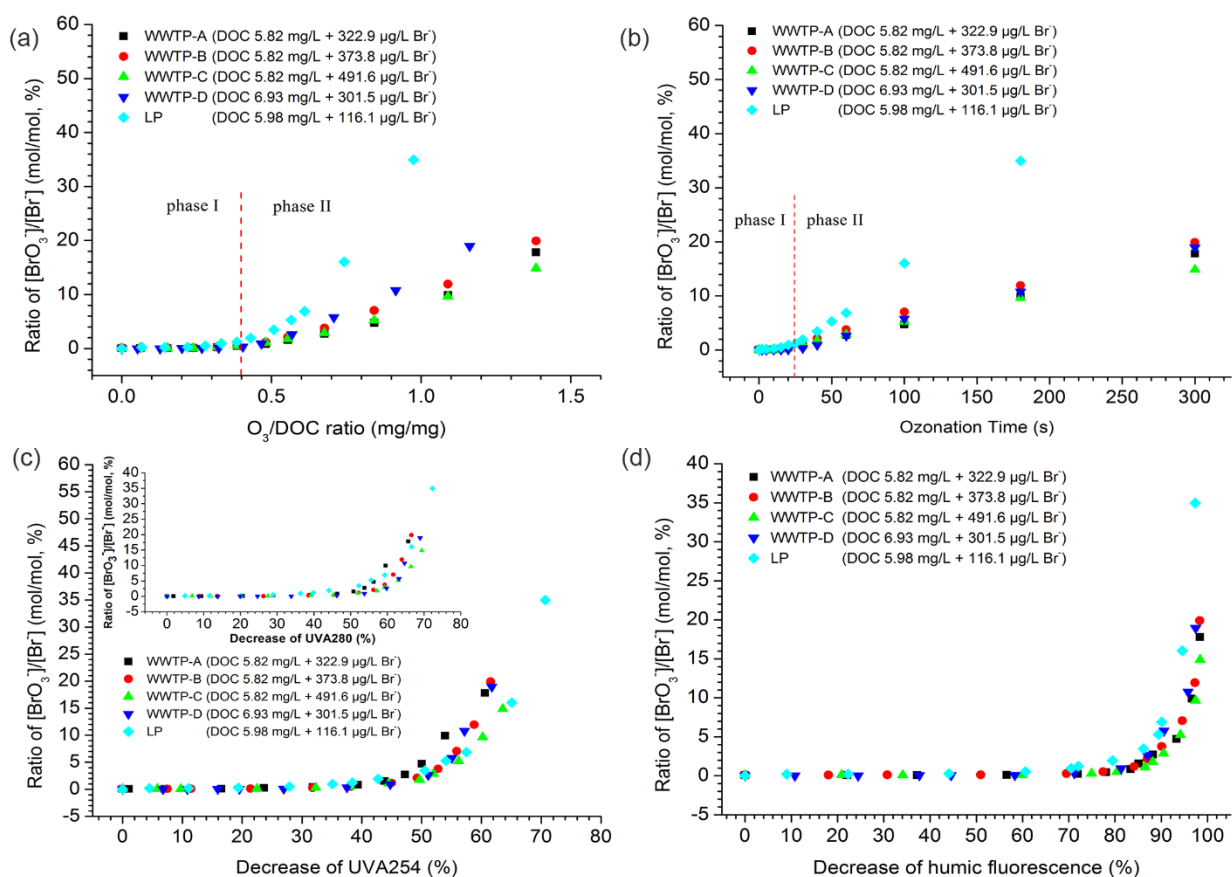


Figure 8

